Apparent thermal contraction of single-walled carbon nanotubes

Guoxin Cao, Xi Chen,* and Jeffrey W. Kysar
Nanomechanics Research Center, Department of Civil Engineering and Engineering Mechanics, Columbia University, New York, New York 10027, USA

(Received 14 June 2005; revised manuscript received 30 August 2005; published 1 December 2005)

The thermomechanical behavior of single-walled carbon nanotubes (SWCNTs) is governed by the competition between quasistatic thermal expansion and dynamic thermal vibration, while the vibration effect is more prominent and induces apparent contraction in both radial and axial directions. We perform extensive molecular-dynamics simulations to explore the mechanisms of thermal expansion and apparent contraction of SWCNTs. The contributions of various vibration modes to apparent thermal contraction are analyzed explicitly at different temperatures. Parallel continuum analyses are also used to validate the vibration characteristics.

DOI: 10.1103/PhysRevB.72.235404 PACS number(s): 61.48.+c, 65.80.+n, 61.50.Ah, 81.07.De

I. INTRODUCTION

Single-walled carbon nanotubes (SWCNTs) have great potentials in nanomechanical and electronic devices: the SWCNT-based composites are light-weight structural materials with extraordinary stiffness and strength,[1] and SWCNTs may also be employed in nanoelectronic components as the next generation of semiconductors and nanowires.[2] The thermomechanical properties of nanodevices are of important since the operations of such devices typically require a significant amount of heat to be dissipated in a small region. Upon heating, the residual stress induced by thermal-expansion mismatch between the SWCNT, matrix, and substrate strongly affects the electrical and mechanical properties of the components, thus it is critical to the system reliability. Perhaps the most fundamental thermomechanical property of SWCNTs is the coefficient of thermal expansion (CTE), and it must be fully understood before characterization of the residual stress in each component caused by CTE mismatch.

By using x-ray diffraction on a SWCNT cluster, negative and positive axial CTEs have been found at low and high temperatures, respectively.[3,4] Experiments on the CTE of a single SWCNT are difficult and such data are still lacking. Numerical analyses based on molecular-dynamics (MD) simulation therefore provide useful insights into the thermomechanical behaviors of SWCNTs. With increase of temperature, if the SWCNT remains *quasistatic*, the bond length elongation induced by internal energy would lead to thermal expansion in both axial and radial directions.[5] On the other hand, increase of structural and vibrational entropy with heating causes *dynamic* thermal vibration in the system with characteristic frequencies, which leads to apparent thermal contraction if one measures the axial distance between the two ends of SWCNTs.[6] The effect of lateral vibration on the apparent thermal axial contraction is sketched in Fig. 1. Ultimately, *the morphology of SWCNTs at any finite temperature is a superposition of both quasistatic and dynamic components*. It is of fundamental value to understand the competition between thermal expansion and vibration (contraction) behaviors, as well as the contributions of various vibration modes in radial, axial, and lateral directions. In addition, to overcome the length and time scale limits of MD simulation, simple continuum-based models with effective properties which closely duplicate the atomistic simulation are needed.

In this paper, we perform extensive numerical studies on both thermal-expansion and vibration characteristics of SWCNTs. Various vibration modes are decoupled, and the mechanisms of apparent thermal contraction are explored by investigating the contributions of each mode. A simple continuum beam model is used to predict the vibration frequencies, and parallel simulation based on the finite element method (FEM) is compared with MD analyses.

II. NUMERICAL APPROACH

Atomic interactions in the SWCNT system are modeled by using the CVFF (consistent valence force field),[7] where the bond-bond stretching energy is expressed by the anharmonic Morse potential. With CVFF, both vibration amplitude and equilibrium distance between atoms increase with heating, thus making it possible to simulate thermal expansion. Since periodic boundary conditions may introduce spurious phonon modes and constrain certain modes of vibration, in this study, an open-ended (5,5) SWCNT is employed in MD simulation. At temperature 0 K, the SWCNT is initially straight with undeformed total length $L_0=24.4$ nm between its open ends. In order to remove the dangling-bond effect,

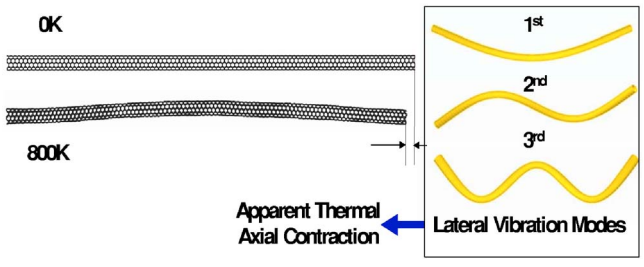

FIG. 1. (Color online) The apparent thermal axial contraction of SWCNTs is caused in part by the lateral vibration modes through bending coupling, and in part by random lattice thermal vibration [Fig. 2(b)]. The SWCNT configuration at 800 K is computed from MD analysis, whereas the shapes of lateral vibration modes are obtained from continuum analyses [Eq. (1)].

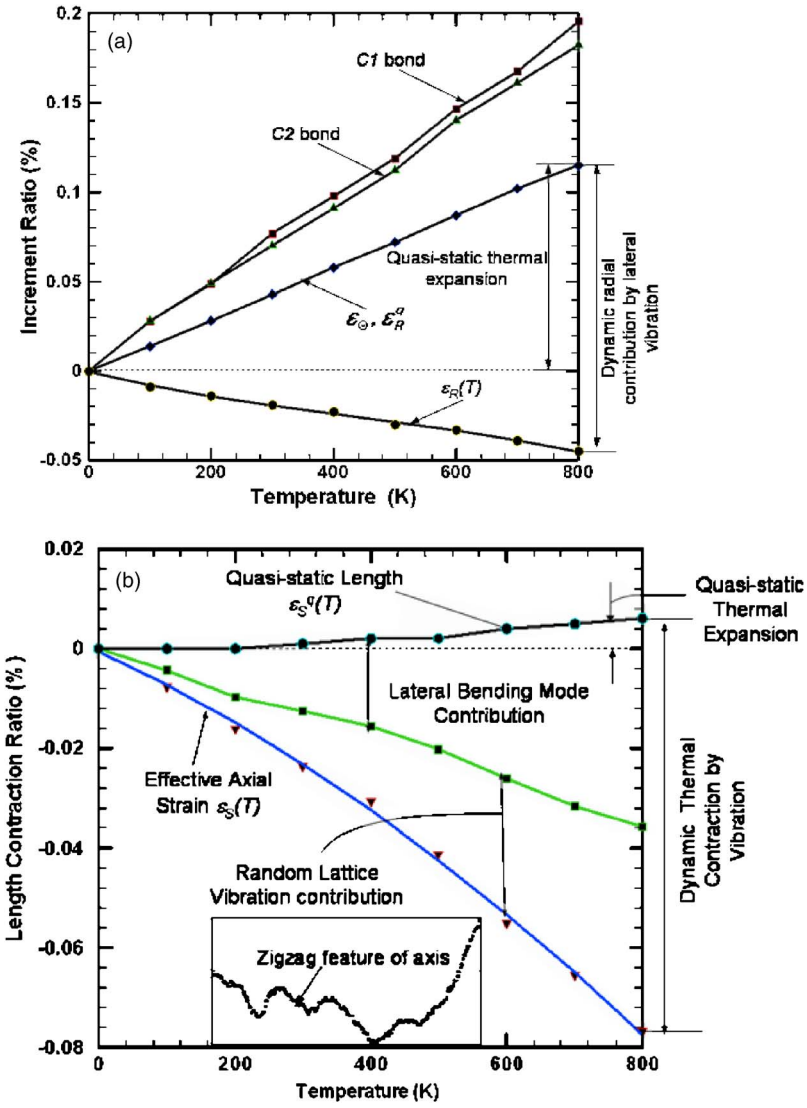

FIG. 2. (Color online) Quasistatic thermal expansion vs dynamic contraction by vibration modes: (a) Bond length elongation and thermal expansion and contraction behaviors in radial direction. (b) Thermal expansion and contraction behaviors in axial direction.

20 terminating layers of carbon atoms on each end are ignored when evaluating the undeformed and deformed lengths in the axial direction, which gives an undeformed axial length of the segment, $S_0=19.77$ nm. The radius of undeformed circular cross section is $R_0=0.338$ nm.

The temperature field is varied from $T=100$–800 K with an increment of 100 K. At each desired T, 100 000 MD equilibration steps (with a fixed time step 1 fs) is carried out until the system has reached a constant temperature. The SWCNT morphology is recorded in the next 500 ps and averaged over this period. The following variables are used to describe the deformed shape, from which thermal expansion and contraction behaviors may be derived: (i) the apparent axial length of the segment along the direction of undeformed axis $S(T)$, which may also be measured from experiments; (ii) the effective radius $R(T)$, which is the average distance of each atom from the center of mass of that layer, then averaged over all layers; (iii) the circumferential length $\Theta(T)$, which is the summation of distances between neighboring atoms in a layer, then averaged over the entire SWCNT. The variation ratios of S, R, and Θ are the effective axial strain (ε_S), effective radial strain (ε_R), and circumferential strain (ε_Θ), respectively. In all cases, rigid body motions have been subtracted off from the motion of the nanotube.

The quasistatic thermal-expansion behavior arises from stretching of C1 (circumferential) and C2 (axial) bonds. The average increment ratios of C1 and C2 bonds are given in Fig. 2(a). The circumferential length of the nanotube $\Theta(T)$ is essentially independent of vibration modes. From Fig. 2(a), ε_Θ increases almost linearly with heating, which is identical to the quasistatic component of effective radius ε_R^q. ε_Θ is about 60% of the stretching strain of C1 or C2 bonds, due to the effect of bond angle variation. On the other hand, the quasistatic expansion of SWCNT in the axial direction can be calculated as the length of deformed center axis, which is the summation of distances between geometric centers of adjacent layers. The quasistatic axial strain ε_S^q is positive thanks to C2 bond elongation. Similar to the circumferential strain, the quasistatic axial strain is smaller than the increment ratio of C-C bonds due to both in-plane and out-of-plane bond angle adjustment. When compared with the overall effective axial strain ε_S (negative at $T=100$–800 K) in Fig. 2(b), it can be seen that the effects of dynamic thermal

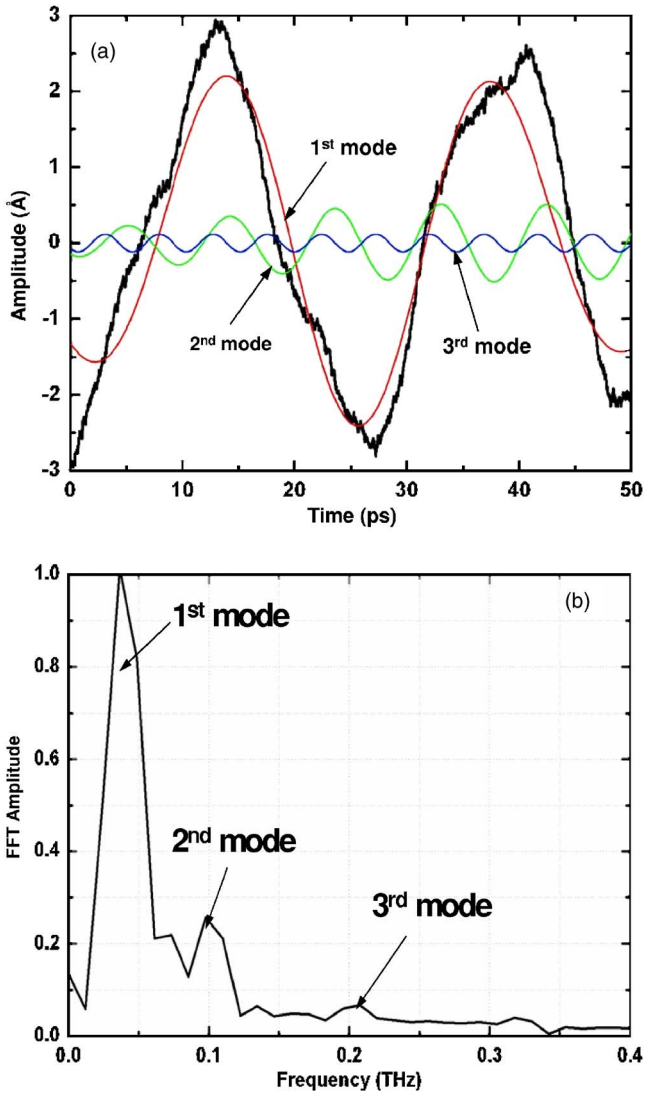

FIG. 3. (Color online) (a) Time history of amplitude, (b) FFT of lateral vibration of the geometric center of middle section at 800 K. The lateral frequencies are robust for other sections and temperatures.

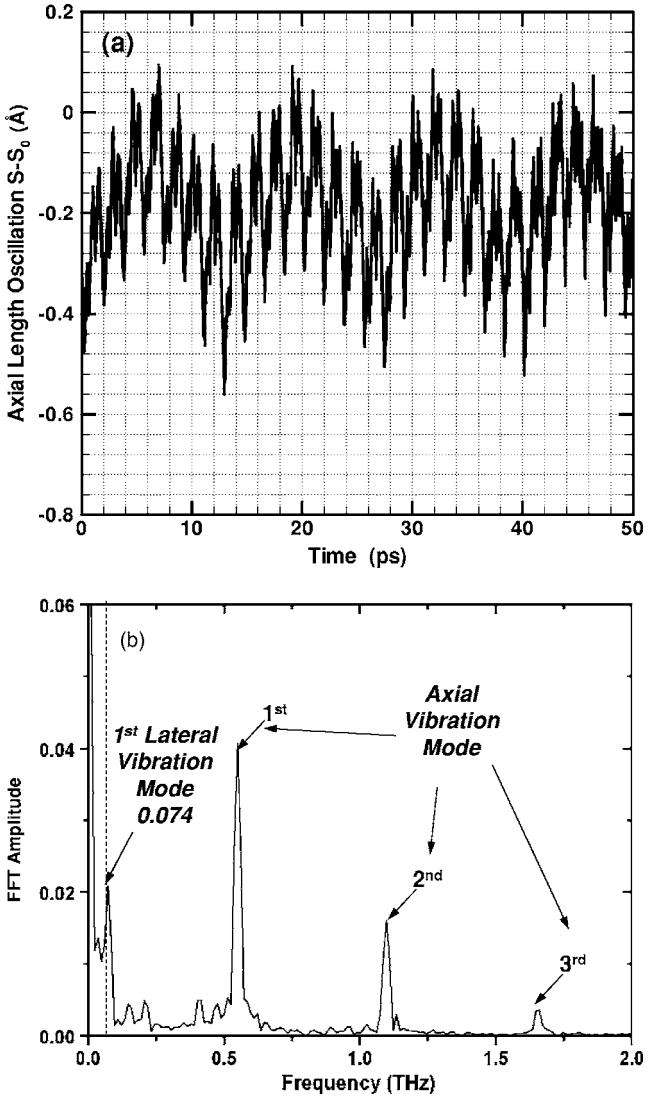

FIG. 4. (a) Time history of amplitude. (b) FFT of oscillation of apparent axial length at 800 K. The low frequency comes from lateral vibration and high frequencies belong to axial vibration.

vibrations have overcome the quasistatic bond elongation, which leads to *apparent thermal axial contraction* (cf. Fig. 1) and *negative axial CTE*. The most important dynamic contributions come from beamlike lateral vibration and random thermal lattice vibration, analyzed below.

The lateral vibration modes and frequencies may be explored from the lateral displacement (vibration amplitude) histories of the geometric center of atomic layers. A typical example is given in Fig. 3(a) for the center layer at 800 K. From fast Fourier transform (FFT) analysis [Fig. 3(b)], frequencies 0.037, 0.104, 0.208, and 0.328 THz can be identified—they correspond to the four lowest lateral natural vibration frequencies of the SWCNT. The overall lateral vibration behavior may be approximated as the superposition of these lowest lateral natural vibration modes (Fig. 1) with varying amplitude [Fig. 3(a)]. From extensive MD analyses, it is found that the lateral vibration frequencies are robust for all layers and remain essentially unchanged at all temperatures. With varying T, there is no new vibration mode or frequency activated; instead, only the overall vibration amplitude increases.

Lateral vibration causes SWCNTs to bend at finite temperature, which is responsible for part of the apparent contraction in SWCNTs. The time history of the variation of apparent axial length $S(T)-S_0$ is given in Fig. 4(a) at $T=800$ K: it is apparent that the oscillation of $S(T)$ is a superposition of a low-frequency vibration mode plus several high-frequency vibration modes. Indeed, from FFT analysis in Fig. 4(b), the low frequency 0.074 THz and high frequencies 0.55, 1.10, and 1.65 THz can be found. The low frequency, 0.074 THz, is exactly twice the frequency of the first mode of lateral natural vibration [0.037 THz, Fig. 3(b)]. It is straightforward to show that when the lateral bending vibration is projected into the axial direction, its frequency is doubled. On the other hand, the high frequencies of $S(T)$ [Fig. 4(b)] do not appear in the frequency spectrum of lateral vibration [Fig. 3(b)], thus they are due to axial vibration.

When averaged over a long period, $S(T)-S_0$ is negative, indicating apparent thermal contraction which is consistent with Fig. 2(b).

The frequencies can be explained via continuum analysis. As a complementary approach to MD, the SWCNTs may be conveniently modeled as continuous cylindrical shells[8] with a fixed wall thickness t and a fixed Young's modulus E—the only variable used to distinguish different chiralities is the radius of the undeformed shell R_0. By computing the strain energies of tension, bending, and torsion for nine SWCNTs with different chirality, comparisons between MD and continuum studies lead to a set of parameters, $E \cong 6.85$ TPa and $t \cong 0.08$ nm, that are within 5% error for all deformation modes and for all SWCNTs.[9] The Young's modulus does not vary significantly with temperature[5] and it is assumed to be a constant from 0 to 800 K in this study. Since the aspect ratio L_0/R_0 is very large, the SWCNT may be regarded as a beam with the same section and elastic property,[9] where analytical results for the modes and natural frequencies of vibration are readily available. Denote the deformed shape of the beam as $W(z)$ (with z the axial coordinate), for a beam with free ends and undeformed length L_0, the profiles of the several lowest lateral vibration modes are[10]

$$W_n(z) = D_n[(\cosh\alpha + \cos\alpha) + (\cos\beta - \cosh\beta)(\sinh\alpha + \sin\alpha)/(\sinh\beta - \sin\beta)], \quad (1)$$

where D_n is the vibration amplitude of the nth mode ($n=1,2,3,\ldots$), $\alpha=k_n z$, and $\beta=k_n L_0$. k_n is the nth eigenvalue given by $k_1L_0=4.730$, $k_2L_0=7.853$, $k_3L_0=10.996$, and $k_4L_0=14.14$. The three lowest natural vibration modes are sketched in Fig. 1. The characteristic frequencies of the several lowest modes of lateral vibration are

$$f_n = \sqrt{EI/(\rho A)}(k_n L_0)^2/(2\pi L_0^2), \quad (2)$$

where $A=2\pi R_0 t$ is the beam cross-section area, $I=\pi R_0 t(4R_0^2+t^2)/4$ is the moment of inertia, and ρ is the density. Assuming the mass of SWCNT is distributed uniformly along the beam ($\rho=9517$ kg/m^3), the four lowest lateral vibration frequencies of (5,5) SWCNTs are 0.038, 0.107, 0.210, and 0.348, respectively—these values are very close to that obtained from MD analyses [Fig. 3(b)], which have also validated the beam model along with its continuum parameters ($E \cong 6.85$ TPa and $t \cong 0.08$ nm).[11]

The axial vibration of the beam is harmonic, which causes the ends of beam to vibrate around their equilibrium positions and *has no net contribution to the apparent length* (or contraction). The natural frequencies of the several lowest axial vibration modes are

$$\omega_n = (n/2L_0)\sqrt{E/\rho} \quad (n = 1,2,3,\ldots). \quad (3)$$

For (5,5) SWCNTs, $\omega_1=0.55$ THz and $\omega_1=1.12$ THz, which are in excellent agreement with MD findings [Fig. 4(b)].

The contribution of lateral bending vibration on apparent thermal contraction may also be estimated from the beam model. For each mode n, the lateral vibration amplitude D_n in Eq. (1) may be obtained from MD analyses [e.g., Fig. 3(a)]. Therefore if the axial length of the beam were to remain a constant L_0 during vibration, the apparent contraction ratio caused by the bending effect can be estimated by adding up the contributions from several lowest lateral vibration modes; the result is plotted in Fig. 2(b). The lateral bending effect is responsible for about half of the reduction of apparent axial length. It should be noted that the apparent axial contraction also depends on the length and radius of the nanotube, where the longer and thinner tube exhibits more flexible beamlike behavior and thus contracts more in the axial direction. Since the energy of each phonon (vibrational mode) scales with kT (where k is the Boltzmann's constant), the average lateral vibration amplitude scales with $D_n \sim kTL^3/(EI)$.[12,11] Hence the axial contraction caused by the lowest lateral vibration mode is estimated to be $\sim D_1^2/L \sim kTL^2/(EI) \sim kTL^2/(ER_0^3 t)$ when $t \sim R_0$. This scaling relationship clearly shows that more axial contraction is favorable for longer and thinner SWCNTs. Since the chirality is only exhibited through the radius of the tube in the continuum model, one would expect to observe more axial contraction caused by lateral bending in SWCNTs with smaller diameter, e.g., (4,4) or (3,3). When added together, the lateral vibration modes, which are low-frequency, long-wavelength mechanical phonons, contribute to about one-half of the total apparent contraction in the axial direction.

The other half of apparent thermal contraction is due to the random thermal lattice vibration (or high-frequency, short-wavelength thermal phonons). At finite T carbon atoms vibrate randomly around their equilibrium positions with a frequency of about 30 THz, which is much higher and also independent of the system vibration modes. The lattice vibration causes the geometric center of each atomic layer to differ slightly from its ideal position, leading to a rough center axis. To illustrate, the morphology of the center axis at 800 K and 20 ps is shown in the inset in Fig. 2(b) (not drawn to scale). The zigzag features in the deformed shape help to further reduce the apparent axial length of the SWCNT.

Dynamic lateral vibration also causes apparent radial contraction through bending coupling. Such effect is shown in Fig. 2(a) as the difference between the quasistatic component of effective radius ε_R^q and overall effective radius ε_R. The FFT of time history of radial oscillation $R-R_0$ of the center layer at 800 K is given in Fig. 5, where two main frequencies can be identified: a lower frequency about 0.037 THz [Fig. 5(a)] which is identical to the lowest lateral natural vibration mode [Fig. 2(b)]; and a higher frequency about 13.5 THz [Fig. 5(b)], which is very close to the radial breathing mode (RBM) of SWCNTs.[5]

The lowest lateral vibration mode causes SWCNTs to bend into a shape which approximates one-half period of a sinusoidal wave. Consequently, the cross section of the nanotube changes from circular to slightly elliptical and the effective radius R is reduced, leading to an apparent contraction in the radial direction. An example is shown in the inset of Fig. 5(a) at $T=800$ K at a particular time instant (with the largest possible difference with respect to the unperturbed circular configuration at 0 K; such difference has been magnified 100 times).

The RBM is generally considered to be harmonic[5] and has essentially no contribution to the effective radial strain. Kwon *et al.*[6] have also reported a pinch mode and a twist mode for the thermal vibration of SWCNTs, which are not

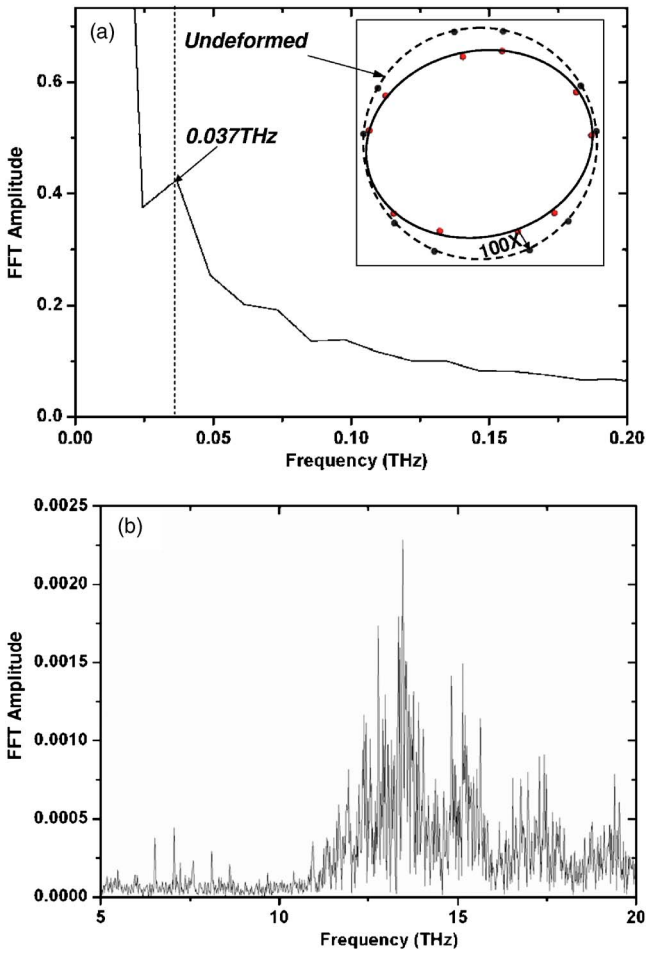

FIG. 5. (Color online) FFT results show (a) low frequency, (b) high frequency of radial vibration at 800 K. The low frequency comes from lateral vibration (which changes cross section to elliptical) and high frequencies belong to axial vibration.

observed in the present study. The pinch mode becomes significant only in thin shells, which requires the SWCNT to be short *and* with a large radius[9]—both not applicable to the long, beamlike SWCNT adopted in this paper. The effect of aspect ratio and section ratio on thermal vibration properties is beyond the scope of current paper; such work is in progress and will be published elsewhere. The twist mode is active only in nanotube bundles[6] and does not exist in this study.

In order to overcome the limits of length and time scales in MD analyses, the continuum approach is sometimes desirable. As discussed earlier, the beam model has been successfully employed to predict the lateral and axial vibration frequencies of SWCNTs. Moreover, we have performed FEM simulations on the vibration behaviors of SWCNTs, where several lowest vibration modes may be activated simultaneously. In FEM simulation, the SWCNT is modeled as a continuous shell with the aforementioned geometry and elastic property. To launch vibration, initial velocities are imposed on the nodes such that the steady-state vibration amplitudes are roughly equal to that obtained in MD in all directions. Comparison between the lateral and axial vibration characteristics obtained from MD and FEM analyses (at

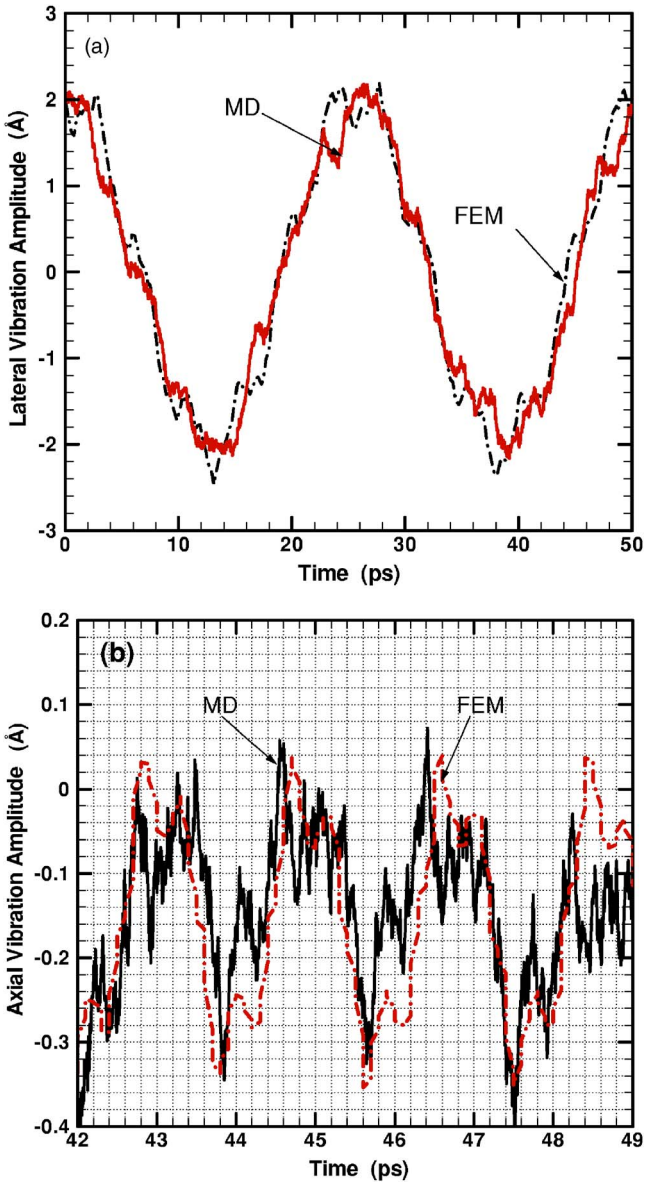

FIG. 6. (Color online) The time history of the geometric center of the middle layer of SWCNTs: comparison between MD and FEM simulations at 800 K. (a) lateral vibration; (b) axial vibration.

800 K) are given in Figs. 6(a) and 6(b), respectively. From FFT analyses, the lateral frequencies 0.037, 0.106, 0.209, and 0.339 THz, and axial frequencies 0.55, 1.12, and 1.67 THz are found from FEM—all in excellent agreement with MD [Fig. 3(b) and 4(b)]. Furthermore, the lateral and axial vibration modes may be readily decoupled in FEM analyses by setting certain initial velocity components to zero. The FEM studies have verified that the axial oscillation has no net contribution to the apparent thermal axial contraction.

III. CONCLUSION

In summary, a systematic and relatively complete MD investigation is carried out to analyze both thermal expansion and apparent contraction behaviors, and to obtain explicit

information on various vibration modes as well as their quantitative contributions to the apparent contractions in axial and radial directions. The quasistatic thermal expansion and dynamic thermal vibration are decoupled quantitatively via extensive MD analyses, as well as the relevant thermal vibration modes in both axial and radial directions. We have also carried out continuum studies to verify the thermal vibration frequencies and show that continuum simulation effectively reproduces the dynamic behaviors of SWCNTs. It is found that the quasistatic thermal expansion of SWCNTs is initiated by C-C bond elongation, whereas the dynamic thermal vibration has reduced both the effective radius and apparent axial length. At any finite temperature, the apparent CTEs in axial and radial directions are negative, and they may be readily derived from Fig. 2.

The radial contraction is primarily caused by the lowest lateral vibration mode via bending coupling, which changes the tube cross section into slightly elliptical shape. On the other hand, the reduction of apparent axial length is caused in part by the bending effect of lateral vibration modes (Fig. 1), and in part by the random thermal lattice vibration. The axial vibration modes have no net effect on the apparent axial length. All lateral and axial vibration frequencies obtained from MD simulation agree very well with beam theory and FEM simulation. Thus the continuum analyses may be used to study the vibration frequencies of SWCNTs and to simulate thermal vibration behaviors. Although specified for SWCNTs with both ends free, the general MD and continuum approaches may be readily extended to SWCNTs with other boundary conditions and such work is in progress.

Ultimately, the thermomechanical behavior of SWCNTs is exhibited through the competition between quasistatic thermal expansion and dynamic thermal vibration; the latter is more prominent and causes apparent thermal contraction in both radial and axial directions, at least for temperatures below 800 K. Although the studies in this paper are based on (5,5) SWCNTs, the success of continuum modeling makes it possible to extend the main findings in this paper to long SWCNTs with any radius. In particular, the effects of SWCNT length and radius are also estimated via continuum analysis. The studies in this paper may provide useful information to the thermomechanical integrity of CNTs, and become important in practical applications involving finite temperature.

ACKNOWLEDGMENTS

We acknowledge support by the Academic Quality Fund from Columbia University, a MRSEC Seed Grant from Columbia MRSEC NSF No. DMR-0213574, and NSF Grant Nos. CMS-0407743 (X.C.) and CMS-0134226 (J.W.K.).

*Electronic address: xichen@civil.columbia.edu

[1] E. T. Thostenson, Z. Ren, and T.-W. Chou, Compos. Sci. Technol. **61**, 1899 (2001).

[2] R. S. Friedman, M. C. McAlpine, D. S. Ricketts, D. Ham, and C. M. Lieber, Nature (London) **434**, 1085 (2005).

[3] Y. Maniwa, R. Fujiwara, H. Kira, H. Tou, H. Kataura, S. Suzuki, Y. Achiba, E. Nishibori, M. Takata, M. Sakata, A. Fujiwara, and H. Suematsu, Phys. Rev. B **64**, 241402(R) (2001).

[4] Y. Yosida, J. Appl. Phys. **87**, 3338 (2000).

[5] N. R. Raravikar, P. Keblinski, A. M. Rao, M. S. Dresselhaus, L. S. Schadler, and P. M. Ajayan, Phys. Rev. B **66**, 235424 (2002).

[6] Y.-K. Kwon, S. Berber, and D. Toma'nek, Phys. Rev. Lett. **92**, 015901 (2004).

[7] P. Dauber-Osguthorpe, V. A. Roberts, D. J. Osguthorpe, J. Wolff, M. Genest, and A. T. Hagler, Proteins: Struct., Funct., Genet. **4**, 31 (1988).

[8] B. I. Yakobson, C. J. Brabec, and J. Bernholc, Phys. Rev. Lett. **76**, 2511 (1996).

[9] X. Chen and G. Cao (unpublished).

[10] W. Thomson, *Theory of Vibration with Application* (Prentice-Hall, Englewood Cliffs, NJ, 1998).

[11] It should be noted that the continuum frequency could not agree well with MD if other Young's moduli and thickness are chosen. For instance, if $t=0.34$ nm and $E=1$–2 TPa (both are widely adopted in literature) were used from Eq. (2), the lateral vibration frequencies would be underestimated by about 45–60 %.

[12] A. Krishnan, E. Dujardin, T. W. Ebbesen, P. N. Yianilos, and M. M. J. Treacy, Phys. Rev. B **58**, 14013 (1998).